The Time Evolution of Gaps in Tidal Streams

Helmi, Amina; Koppelman, Helmer H.

Published in:
Astrophysical Journal Letters

DOI:
10.3847/2041-8205/828/1/L10

Publication date:
2016

The Astrophysical Journal Letters, 828:L10 (5pp), 2016 September 1 doi:10.3847/2041-8205/828/1/L10

THE TIME EVOLUTION OF GAPS IN TIDAL STREAMS

Amina Helmi and Helmer H. Koppelman
Kapteyn Astronomical Institute, University of Groningen, P.O. Box 800, 9700 AV Groningen, The Netherlands; ahelmi@astro.rug.nl
Received 2016 June 28; revised 2016 August 1; accepted 2016 August 2; published 2016 August 29

ABSTRACT

We model the time evolution of gaps in tidal streams that are caused by the impact of a dark matter subhalo, while these orbit a spherical gravitational potential. To this end, we make use of the simple behavior of orbits in action-angle space. A gap effectively results from the divergence of two nearby orbits whose initial phase-space separation is, for very cold thin streams, largely given by the impulse induced by the subhalo. We find that in a spherical potential, the size of a gap increases linearly with time for sufficiently long timescales. We have derived an analytic expression that shows how the growth rate depends on the mass of the perturbing subhalo, its scale, and its relative velocity with respect to the stream. We have verified these scalings using *N*-body simulations and find excellent agreement. For example, a subhalo of mass $10^8\,M_\odot$ directly impacting a very cold thin stream on an inclined orbit can induce a gap that may reach a size of several tens of kiloparsecs after a few gigayears. The gap size fluctuates importantly with phase on the orbit, and it is largest close to pericenter. This indicates that it may not be fully straightforward to invert the spectrum of gaps present in a stream to recover the mass spectrum of the subhalos.

Key words: dark matter – Galaxy: halo – Galaxy: kinematics and dynamics – Galaxy: structure

1. INTRODUCTION

A key prediction of the concordance cold dark matter model of structure formation is the presence of myriads of dark satellites orbiting the halos of galaxies like the Milky Way (Klypin et al. 1999; Moore et al. 1999). The presence of these objects is directly related to the fundamental nature of the dark matter particle, hence it is of uttermost importance to establish if such subhalos indeed exist, as well as their abundance and properties.

Because such subhalos must be devoid of stars, they are very difficult to detect and the only way, in fact, may be through their gravitational influence. Gravitational lensing is one of the means of detecting their presence, although this technique may be only realistically sensitive to the largest subhalos (Vegetti et al. 2014). A powerful alternative is to measure their impact on the stellar streams orbiting the halos of galaxies (Ibata et al. 2002; Johnston et al. 2002). Streams are effectively composed of stars on very nearby orbits, and hence if a subhalo comes close to such a stream, it will slightly modify the orbits of those stars, leading to a change in its structure and to the formation of a gap (Yoon et al. 2011).

It has been argued that the distribution of gap sizes can be used to infer the mass spectrum of perturbers, and this is a truly interesting prospect (Carlberg 2009; Carlberg & Grillmair 2013; Erkal & Belokurov 2015b; Bovy et al. 2016). Most works so far have explored circular orbits for the streams as they move in a spherical potential (Carlberg 2013; Erkal & Belokurov 2015a, 2015b; Erkal et al. 2016), although Carlberg (2015) has considered the effect of eccentricity on gaps in streams orbiting in a triaxial mass distribution. Most recently, Sanders et al. (2016) modeled the evolution of a gap in a stream on a non-circular orbit in an axisymmetric potential, but their focus was on the behavior in angle and frequency space. At the moment, no simple analytic model exists that can predict how a gap, once formed, evolves with time in *physical* space, and how its characteristics depend exactly on the properties of the subhalo and the encounter. This is in fact the goal of this Letter. It may be seen as an important step toward a full modeling of the gap's spectrum in a cosmological context, for example, along the lines of Erkal et al. (2016).

The paper is organized as follows. In Section 2 we describe the method used to model the evolution of a stream and the *N*-body simulations carried out to validate the approach. In Section 3 we describe the results, and we conclude in Section 4.

2. METHODS

The model we use is based on two ingredients: the use of the impulse approximation, and the divergence of nearby orbits. We describe these ingredients in what follows, and then describe the *N*-body simulations that we have used for validation.

2.1. The Impulse Approximation

The impulse approximation (see chap. 8 of Binney & Tremaine 2008) can be used to determine the perturbation induced by a subhalo on a stream star, as well as its dependence on the properties of the subhalo and the relative motion with respect to the stream.

Here we follow the description by Erkal & Belokurov (2015a), where the stream's velocity at the position of impact with the subhalo is aligned with the *y*-direction, implying that this is also the direction of the stream (locally). The stream moves in the $x - y$ plane with velocity v_y, while the subhalo of mass M_s has a velocity (w_x, w_y, w_z) at the time of impact. For simplicity we assume that the subhalo crosses the stream itself, i.e., the impact parameter is $b = 0$ kpc. Using the impulse approximation, the change in each of the velocity components for stars on the stream v_i can be computed from

$$\Delta v_i = \int_{-\infty}^{+\infty} a_i(x, y, z)\mathrm{d}t,$$

where a_i is the acceleration field in the *i*-direction due to the subhalo on a star located at position (x, y, z). This expression can be computed numerically for any functional form for the subhalo's mass distribution (Sanders et al. 2016) such as, e.g.,

the cosmologically motivated (truncated) NFW (Navarro et al. 1996). However, for a Plummer sphere and assuming the stream is one-dimensional (1D; i.e., x and z are constant), it takes a particularly simple form:

$$\Delta v_x = 2GM_s \frac{y w_\perp w_\parallel \sin\alpha}{w\,(r_s^2 w^2 + w_\perp^2 y^2)}, \quad (1)$$

$$\Delta v_y = -2GM_s \frac{y w_\perp^2}{w\,(r_s^2 w^2 + w_\perp^2 y^2)}, \quad (2)$$

$$\Delta v_z = -2GM_s \frac{y w_\perp w_\parallel \cos\alpha}{w\,(r_s^2 w^2 + w_\perp^2 y^2)}. \quad (3)$$

Here $w_\parallel = v_y - w_y$, $w_x = -w_\perp \sin\alpha$, $w_z = w_\perp \cos\alpha$, and therefore $w_\perp = (w_x^2 + w_z^2)^{1/2}$. It is sometimes argued that Δv_x and Δv_z can be neglected (see, e.g., Yoon et al. 2011); however, in what follows we consider the velocity change in all directions (as in, e.g., Erkal & Belokurov 2015a; Sanders et al. 2016). These expressions show that the velocity kick received by a star depends on its distance from the point of impact, falling off as $1/y$ for sufficiently large distances, and reaching maximum amplitude at

$$y_{\max} = \pm w/w_\perp r_s, \quad (4)$$

with a value

$$\Delta v_y^{\max} = \mp GM_s w_\perp / (w^2 r_s). \quad (5)$$

For a non-zero impact parameter b the last expressions remain similar, with r_s replaced by $(r_s^2 + b^2)^{1/2}$.

2.2. The Divergence of Nearby Orbits

Once a subhalo has given an impulse to stars located in a portion of a stream, these will continue to orbit the host gravitational potential, albeit on slightly modified trajectories. These trajectories will diverge from each other in a fashion that can be described using the action-angle formalism (Helmi & White 1999; Helmi & Gomez 2007).

We can use the behavior of the spatial separation $\Delta\boldsymbol{X}$ of two nearby orbits to actually describe the evolution of a gap. On each side of the gap, we can imagine there being two stars A and B moving on different orbits that are slightly offset in position and velocity largely because of the kick received by the encounter with the subhalo. If their initial separation is $\Delta\boldsymbol{X}_0$ and $\Delta\boldsymbol{V}_0$, this can be expressed in action-angle coordinates as

$$\begin{bmatrix}\Delta\boldsymbol{\Theta}_0 \\ \Delta\boldsymbol{J}_0\end{bmatrix} = M_0 \begin{bmatrix}\Delta\boldsymbol{X}_0 \\ \Delta\boldsymbol{V}_0\end{bmatrix}, \quad (6)$$

where M_0 is the Jacobian matrix of the transformation from physical and velocity space to action-angle space, i.e., $M_0 = \partial(\boldsymbol{\Theta}, \boldsymbol{J})/\partial(\boldsymbol{X}, \boldsymbol{V})$ evaluated at the time of the encounter, or minimum impact parameter, t_0, at the phase-space location of, e.g., star A. Recall that

$$\Delta\boldsymbol{\Theta} = \Delta\boldsymbol{\Theta}_0 + \boldsymbol{\Omega}(\boldsymbol{J})t, \qquad \text{and} \qquad \boldsymbol{J} = \boldsymbol{J}_0,$$

where $\boldsymbol{\Omega}(\boldsymbol{J})$ are the frequencies of motion of, e.g., star A's orbit, or in matrix form

$$\begin{bmatrix}\Delta\boldsymbol{\Theta} \\ \Delta\boldsymbol{J}\end{bmatrix} = \Omega' \begin{bmatrix}\Delta\boldsymbol{\Theta}_0 \\ \Delta\boldsymbol{J}\end{bmatrix}, \quad (7)$$

with

$$\Omega' = \begin{bmatrix} I_3 & \partial\boldsymbol{\Omega}/\partial\boldsymbol{J}\, t \\ 0 & I_3 \end{bmatrix}, \quad (8)$$

where $\partial\boldsymbol{\Omega}/\partial\boldsymbol{J}$ is a 3×3 matrix, also equal to the Hessian of the Hamiltonian. Furthermore, performing a local transformation, we find that at time t

$$\begin{bmatrix}\Delta\boldsymbol{X} \\ \Delta\boldsymbol{V}\end{bmatrix} = M_t^{-1} \begin{bmatrix}\Delta\boldsymbol{\Theta} \\ \Delta\boldsymbol{J}\end{bmatrix}. \quad (9)$$

Combining Equations (6), (7), and (9) we finally obtain

$$\begin{bmatrix}\Delta\boldsymbol{X} \\ \Delta\boldsymbol{V}\end{bmatrix} = M_t^{-1}\Omega' M_0 \begin{bmatrix}\Delta\boldsymbol{X}_0 \\ \Delta\boldsymbol{V}_0\end{bmatrix}, \quad (10)$$

which allows us to measure the physical separation $\Delta\boldsymbol{X}$ at time t between nearby orbits, or in our case, the size of the gap at any point in time.

Let us consider what this predicts for sufficiently long timescales, and for evolution in a spherical potential. In that case, the motion occurs in a plane. This somewhat simplifies the matrices, in the sense that they are either 2×2 or 4×4. The spatial separation is given by $|\Delta\boldsymbol{X}|$ or $(\Delta\boldsymbol{X}^\dagger \Delta\boldsymbol{X})^{1/2}$, and this can be computed by noting that in Equation (8), the dominant submatrix is the upper right one: $[\partial\boldsymbol{\Omega}/\partial\boldsymbol{J}\, t]$. Therefore in Equation (10):

$$\Delta\boldsymbol{X} \sim t\, M_{t,1}^{-1} [\partial\boldsymbol{\Omega}/\partial\boldsymbol{J}] \Delta\boldsymbol{J}_0, \quad (11)$$

where $M_{t,1}^{-1}$ is the upper left submatrix of M_t^{-1}, and transforms from physical to angle coordinates: $\partial\boldsymbol{X}/\partial\boldsymbol{\Theta}$. Therefore

$$|\Delta\boldsymbol{X}| \sim t\,(\Delta\boldsymbol{J}_0^\dagger C_{\boldsymbol{x},\boldsymbol{\Omega}} \Delta\boldsymbol{J}_0)^{1/2}, \quad (12)$$

where $C_{\boldsymbol{x},\boldsymbol{\Omega}} = [\partial\boldsymbol{\Omega}/\partial\boldsymbol{J}](M_{t,1}^{-1})^\dagger M_{t,1}^{-1} [\partial\boldsymbol{\Omega}/\partial\boldsymbol{J}]$ is a symmetric matrix that thus depends on the location of the gap along its orbit and the orbit itself through the frequency derivatives. This equation shows explicitly that the physical separation between nearby orbits, or equivalently, the size of a gap, increases linearly with time for long timescales. Since the matrix $M_{t,1}^{-1}$ depends on the location of the gap at time t, this shows also that the physical size of a gap will vary depending on its orbital phase. From Equation (11) we can also estimate the gap's volume as $\propto \Delta X \Delta Y \propto t^2$ for a non-circular orbit in a spherical potential. More generally, the gap's volume will grow as t^n, with n being the number of independent frequencies (as encoded in the matrix $[\partial\boldsymbol{\Omega}/\partial\boldsymbol{J}]$).

Let us now explore the dependence of gap size on the subhalo mass and size and the conditions of the encounter, all of which are implicit in $\Delta\boldsymbol{J}_0$. The initial action separation depends on $\Delta\boldsymbol{X}_0$ and $\Delta\boldsymbol{V}_0$, but the term that dominates is that associated with the change in velocity (Equation (5)). With the geometry considered for the encounter, it can be shown using Equation (6) that $\Delta\boldsymbol{J}_0 = 2\Delta v_y^{\max} \boldsymbol{f}_{\mathrm{orb},0}$, where $\boldsymbol{f}_{\mathrm{orb},0} = [x_0, (v_{y,0} - x_0\Omega_\phi)/\Omega_r]$, where $v_{y,0}$ is the velocity of the stream at the time and location of the impact and x_0 its x-location. The frequencies Ω_r and Ω_ϕ are the radial and azimuthal frequencies of, e.g., star A. Combining these expressions we find that for sufficiently long timescales, the

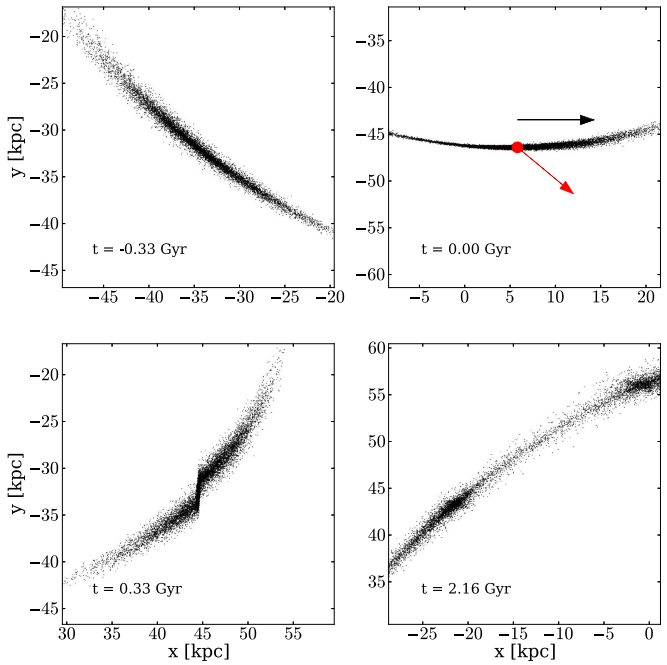

Figure 1. Stream particles, before, during, and after a direct encounter with a dark subhalo of $M_s = 10^{7.5}\,M_\odot$ (red symbol in the top right panel). At late times, a gap, in the form of a significant decrease in density, along the stream is clearly apparent. The arrows indicate the direction of the velocity vectors of the stream (black) and the subhalo (red) at the time of the encounter.

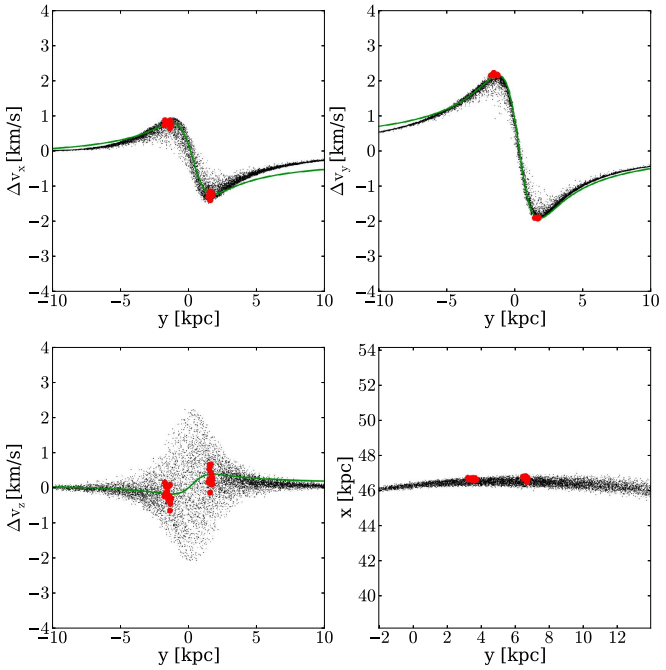

Figure 2. Velocity changes along the stream for the experiment shown in Figure 1. The red particles have been identified as those that have experienced the maximum velocity change. The green curve indicates the prediction using the impulse approximation.

gap size grows as

$$|\Delta \boldsymbol{X}| \sim t\frac{2GM_s w_\perp}{w^2(r_s^2+b^2)}(f^\dagger_{\rm orb,0} C_{\boldsymbol{x},\boldsymbol{\Omega}} f_{\rm orb,0})^{1/2}, \quad (13)$$

while the general expression for the gap's size at any point in time can be exactly determined using Equation (10).

2.3. N-body Simulations

To validate the above analytic description, we have performed N-body simulations of the encounters of a subhalo with a stream orbiting a spherical NFW potential, of virial mass $M_{\rm halo} = 3 \times 10^{11}\,M_\odot$ and scale radius $r_s = 15.6$ kpc.

The progenitor of the stream is initially distributed following a Gaussian in configuration and velocity space, with 1D-dispersions $\sigma_x = 0.05$ kpc and $\sigma_v = 2$ kpc/Gyr (~2.04 km s^{-1}), respectively. It is evolved using GADGET-2 and placed on an eccentric orbit with pericenter $r_p \sim 46$ kpc and apocenter $r_a \sim 71$ kpc, for a total of ~9 Gyr.

At time $t = 2.33$ Gyr the stream experiences an encounter with a subhalo. This is modeled as a rigid Plummer sphere, i.e., we do not use particles to follow its evolution. We have carried out experiments using a range of masses and scale radii ($\log_{10} M_s[\,M_\odot]$, r_s[kpc]) = [(6.9, 0.38), (7.2, 0.59), (7.5, 0.9), (7.9, 1.35)]. All encounters have the same impact parameter $b = 0$ kpc and the subhalo moves with velocity $(w_x, w_y, w_z) = (80.1, 97.3, -23)$ km s^{-1} in the frame in which the stream is on the $x-y$ plane, and the y-direction is aligned with the stream at the time of impact, i.e., this is the configuration used to compute the kicks in Equations (3). At the time and location of the impact, the stream's velocity is 137.1 km s^{-1}.

Figure 1 shows the stream before, during, and after an encounter with a subhalo of mass $M_s = 10^{7.5}\,M_\odot$ and $r_s = 0.9$ kpc. The perturbation induced by the subhalo is apparent, and leads to the formation of a gap that is easily distinguished and extends by more than ~15 kpc only 2 Gyr after the encounter.

3. RESULTS

Figure 2 shows the velocity change experienced by the stream particles at the time of the collision for the experiment in Figure 1. The solid curve corresponds to the predictions from the impulse approximation, i.e., Equations (3), and they reproduce the amplitude and location of the maximum kick received by the stream particles. The deviations at large distances can be attributed to the stream's curvature (see Sanders et al. 2016). The colored points denote "trailing" and "leading" particles, i.e., particles located on either side of the point of impact and that have experienced the maximum velocity change, and which with time, will be on either side of the gap that grows as a result of the encounter.

This is explicitly shown in Figure 3, which depicts the density of the stream in the gaps' vicinity. The vertical lines in this figure indicate the location of the "trailing" and "leading" particles, and show that their separation follows that of the density peaks around the gap at all times. Thus, for computational ease, we measure the gap size using the physical distance between these particles. Such a position (and velocity) difference between two (groups of) star particles could possibly be measurable with *Gaia* and follow-up spectroscopy, allowing direct comparisons to the models. Note that our method to measure the gap's extent differs from that of Erkal & Belokurov (2015a), who used the size of the underdense region. The two methods yield comparable physical extents when applied to our N-body simulations, with the gap size defined by the separation of the particles being only slightly larger, as can be seen from Figure 3.

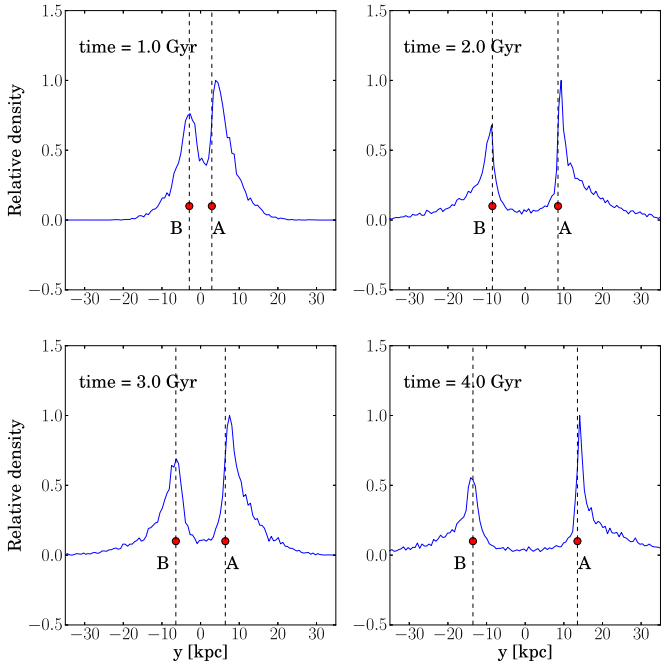

Figure 3. Relative density along the stream around the location of the gap formed in the experiment in Figure 1. The particles *A* and *B* are those that have experienced the maximum velocity change and are used to determine how the gap size evolves with time.

Figure 4 shows the evolution of the gap size produced by subhalos of different masses impacting the stream in the experiments described above. For each experiment, the average separation between pairs of "trailing" and "leading" particles is indicated with the black curve, while the dotted curves correspond to the 1σ scatter. The colored curves in Figure 4 are the predictions obtained using the formalism described in Section 2.2. Each pair of colored curves correspond to the separations $|\Delta \boldsymbol{X}|$ computed through linear perturbations around the orbits of particles initially located on each side of the point of impact (i.e., "stars" *A* and *B* of Section 2.2). We take the initial separation $\Delta \boldsymbol{X}_0$ to be arbitrarily small and in practice we set $\Delta x_0 = \Delta z_0 = 2 \times 10^{-5}$ kpc, while $\Delta y_0 = 2y_{\rm max}$ from Equation (4), in the reference frame aligned with the stream. For the initial velocity separation $\Delta \boldsymbol{V}_0$ we use the prediction from the model, as described in Equation (3) at the maximum. To this impulse-driven velocity change we add a term associated with the velocity gradient $\boldsymbol{\nabla_x V}$ along the stream over the volume Δy_0, which is larger for larger subhalos (as $y_{\rm max}$ depends on r_s). The velocity gradient is not exactly that given by the orbit of, e.g., star *A* (as the stream does not follow a single orbit), but it can be computed using the formalism described in Section 2.2 and in particular using Equation (10) for arbitrary $\Delta \boldsymbol{X}_0$ and $\Delta \boldsymbol{V}_0$. For the stream modeled, the velocity difference due to the gradient is a factor of 2–4 smaller than the impulse received along the direction of motion (but comparable or larger in the other directions) as a consequence of the encounter with the subhalos considered. This of course depends somewhat on the specifics of the stream's progenitor orbit.

As shown in Figure 4 the agreement between the size of the gap measured in the simulations and the predictions of our model is excellent. This implies that we are in a position of

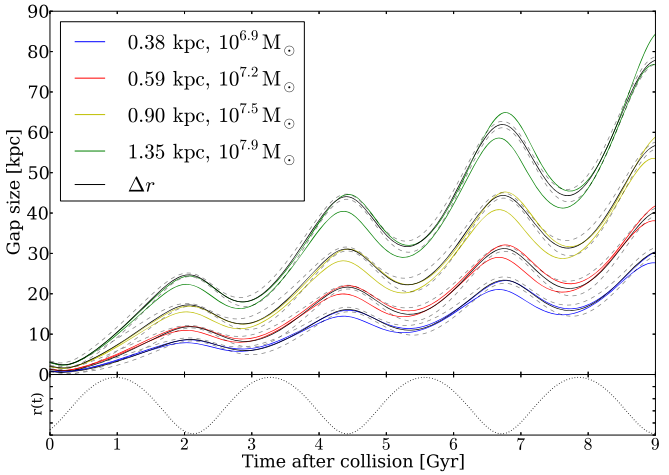

Figure 4. The top panel shows the evolution of the gap size as a function of time for encounters with different subhalos, as indicated in the inset. The agreement between the model predictions and the measured sizes is excellent. The bottom panel shows the radial orbital oscillation and evidence that the size of a gap is largest when this is located close to pericenter.

predicting the size of a gap in a stream for any geometry, subhalo mass, scale, and density profile, at any point in time, for any stream orbiting a spherical potential.

As predicted by our model, the gap size oscillates strongly with time, and comparison to the orbital radial oscillations plotted in the bottom panel of the figure shows that the gap is largest close to pericenter.

4. DISCUSSION

A gap in a stream is essentially the result of the divergence of nearby orbits whose initial separation is driven by an encounter with a dark matter subhalo. This conceptual framework allows us to make detailed predictions for the evolution of gap sizes and their dependence on the properties of the subhalos, the streams, their orbits, and the gravitational potential in which they move.

We have found that, for a spherical potential, gaps can grow very fast, increasing their size linearly with time. Superposed on this long-term behavior, there are important oscillations that depend on their orbital phase. This long-term behavior appears to be in contrast to the $t^{0.5}$ growth proposed by Erkal & Belokurov (2015a) for up to 5 Gyr after the encounter (although, in their simulations, Sanders et al. 2016 also find linear growth at late times). Part of the difference, as mentioned earlier, may lie in the fact that we have considered general orbits instead of only circular orbits. Additionally, differences in the orbital phase of the location of the encounter will lead to different early-time behavior.

The important oscillations in gap size imply that one cannot infer the mass of a subhalo directly from the size of a gap. For example, Figure 4 shows that a gap of 10 kpc size could be induced by a subhalo of mass $M_s \sim 10^{7.9}\,M_\odot$ less than 1 Gyr after impact, but also by a subhalo with $M_s \sim 10^{6.9}\,M_\odot$ but 3.5 Gyr after impact. This degeneracy comes on top of that identified by Erkal & Belokurov (2015b) between the mass of the subhalo M_s and the impact velocity w (Equation (10)). Therefore, inferring the subhalo mass will strongly depend on our ability to determine precisely the orbit of the stream in which the gap is located. We have, however, only focused on

the spatial characteristics of the gap, and not for example, on the kinematical properties, which perhaps can help break some of the degeneracies (see Erkal & Belokurov 2015b). A statistical comparison of the predicted and observed distribution of gap sizes may also be a way to characterize the granularity in the dark matter halos of galaxies (see Carlberg et al. 2012; Bovy et al. 2016; Erkal et al. 2016).

Although the gap size increases linearly with time, the volume it occupies will increase as t^n, with being n the number of independent frequencies of motion. For a general orbit in an arbitrary spherical potential $n = 2$, while for a non-spherical potential there are at most 3 independent frequencies. This means that in this case, gaps may be more apparent since their internal densities will be lower. The model we have developed is sufficiently general that it can be applied in a statistical sense for an ensemble of cosmologically motivated orbits and subhalo mass functions, an idea recently put forward by Erkal et al. (2016). This will allow us to make predictions specific to the ΛCDM model for the spectrum of sizes of stream gaps for direct comparison to observations.

A.H. was partially supported by an NWO-VICI grant. We are grateful to the referee for a constructive report, to Facundo Gómez and Hans Buist for their contribution to improving earlier versions of the software used for this Letter, and to Tjitske Starkenburg for helping us set up the *N*-body simulations.

REFERENCES

Binney, J., & Tremaine, S. 2008, Galactic Dynamics (2nd ed.; Princeton, NJ: Princeton Univ. Press)
Bovy, J., Erkal, D., & Sanders, J. L. 2016, MNRAS, submitted (arXiv:1606.03470)
Carlberg, R. G. 2009, ApJL, 705, L223
Carlberg, R. G. 2013, ApJ, 775, 90
Carlberg, R. G. 2015, ApJ, 808, 15
Carlberg, R. G., & Grillmair, C. J. 2013, ApJ, 768, 171
Carlberg, R. G., Grillmair, C. J., & Hetherington, N. 2012, ApJ, 760, 75
Erkal, D., & Belokurov, V. 2015a, MNRAS, 450, 1136
Erkal, D., & Belokurov, V. 2015b, MNRAS, 454, 3542
Erkal, D., Belokurov, V., Bovy, J., & Sanders, J. L. 2016, MNRAS, in press (arXiv:1606.04946)
Helmi, A., & Gomez, F. 2007, arXiv:0710.0514
Helmi, A., & White, S. D. M. 1999, MNRAS, 307, 495
Ibata, R. A., Lewis, G. F., Irwin, M. J., & Quinn, T. 2002, MNRAS, 332, 915
Johnston, K. V., Spergel, D. N., & Haydn, C. 2002, ApJ, 570, 656
Klypin, A., Kravtsov, A. V., Valenzuela, O., & Prada, F. 1999, ApJ, 522, 82
Moore, B., Ghigna, S., Governato, F., et al. 1999, ApJL, 524, L19
Navarro, J. F., Frenk, C. S., & White, S. D. M. 1996, ApJ, 462, 563
Sanders, J. L., Bovy, J., & Erkal, D. 2016, MNRAS, 457, 3817
Vegetti, S., Koopmans, L. V. E., Auger, M. W., Treu, T., & Bolton, A. S. 2014, MNRAS, 442, 2017
Yoon, J. H., Johnston, K. V., & Hogg, D. W. 2011, ApJ, 731, 58